MR Safe Robotic Manipulator for MRI-Guided Intracardiac Catheterization

Kit-Hang Lee, Kin Chung Denny Fu, Ziyan Guo, Ziyang Dong, Martin C. W. Leong, Chim-Lee Cheung, Alex Pui-Wai Lee, Wayne Luk, *Fellow, IEEE*, and Ka-Wai Kwok

***Abstract*—This paper introduces a robotic manipulator to realize robot-assisted intracardiac catheterization in magnetic resonance imaging (MRI) environment. MRI can offer high-resolution images to visualize soft tissue features such as scars or edema. We hypothesize that robotic catheterization, combined with the enhanced monitoring of lesions creation using MRI intraoperatively, will significantly improve the procedural safety, accuracy, and effectiveness. This is designed particularly for cardiac electrophysiological (EP) intervention, which is an effective treatment of arrhythmia. We present the first MR Safe robot for intracardiac EP intervention. The robot actuation features small hysteresis, effective force transmission, and quick response, which has been experimentally verified for its capability to precisely telemanipulate a standard clinically used EP catheter. We also present timely techniques for real-time positional tracking in MRI and intraoperative image registration, which can be integrated with the presented manipulator to improve the performance of teleoperated robotic catheterization.**

***Index Terms*—MR image registration, MR Safe robot, positional tracking in magnetic resonance imaging (MRI), robot-assisted intervention.**

I. Introduction

CATHETERIZATION involves dexterous manipulation of thin and flexible medical-grade instruments to pinpoint target anatomy for biopsy, drug delivery, or lesion ablation through the transluminal, intraluminal, intracavitary, or intracranial surgical approach. Such surgical manipulation could be applied to cardiovascular intervention, prostate surgery, stereotactic neurosurgery, or breast biopsy. Cardiovascular diseases, which remain the major cause of mortality in developed countries, particularly demand dexterous catheterization. Heart rhythm disorder (known as arrhythmia) is a typical example, to which cardiovascular electrophysiology (EP) is known as an effective surgical treatment [1], [2]. In the procedure, electrophysiologists insert a long catheter mostly from the femoral vein to the heart chamber, in which radiofrequency (RF) ablation is performed at the catheter tip in contact with lesion tissue to isolate the abnormal electrophysiological signals that cause arrhythmias.

Even with catheter navigation using a cardiac EP roadmap, manipulating the catheter to the desired location remains challenging due to the inconsistent control of a thin $\phi < (3\,\text{mm})$, long ($\approx$1.5 m), flexible EP catheter within rapidly deforming cardiovascular tissue, such as the left ventricle (LV) and left atrium (LA). This challenge has drawn attention to the development of teleoperated robotic platforms, including well-known commercial platforms such as Hansen Sensei X and Amigo Remote Catheter System. These platforms aim to improve the dexterity and accuracy of catheter manipulation for intracardiac EP intervention.

Apart from dexterous maneuvering of cardiac catheters to the target tissues, both for electroanatomical (EA) mapping (EP's diagnostic phase) and then RF ablation, the ability to intraoperatively assess lesion locations and their ablation progress is another very crucial factor to enhance the safety and efficacy of the EP procedure. Magnetic resonance imaging (MRI) is a unique image modality capable of offering excellent image contrast for cardiovascular soft tissues, forming a three-dimensional (3-D) cardiac roadmap online. Additionally, MRI-guided EP avoids exposing patients and clinicians to harmful radiation as generated by X-ray and computed tomography in conventional EP procedures. Late gadolinium enhancement T2-weighted cardiac MRI [3] can also readily visualize the physiological change of tissues, and identify the scars or edema arising from successful or incomplete RF ablation. Many research groups (e.g., [4]–[7]) have already conducted numerous patient trials and demonstrated the significant clinical value with the use of intraoperative (intra-op) MRI for EP in clinical routines.

Manuscript received April 20, 2017; revised September 6, 2017 and November 22, 2017; accepted January 21, 2018. Date of publication February 6, 2018; date of current version April 16, 2018. Recommended by Technical Editor D. Stoianovici. This work was supported in part by the Croucher Foundation, in part by the Research Grants Council of Hong Kong (17202317, 17227616, and 27209515), in part by the U.K. Engineering and Physical Sciences Research Council (EP/P010040/1, EP/N031768/1, EP/L016796/1, and EP/L00058X/1), in part by the European Union Horizon 2020 Research and Innovation Programme (671653), in part by Aptorum Group Limited, and in part by Signate Life Sciences Limited. *(Kit-Hang Lee and Kin Chung Denny Fu are joint first authors.) (Corresponding author: Ka-Wai Kwok.)*

K.-H. Lee, K. C. D. Fu, Z. Guo, Z. Dong, M. C. W. Leong, C.-L. Cheung, and K.-W. Kwok are with the Department of Mechanical Engineering, The University of Hong Kong, Hong Kong (e-mail: briankhl@connect.hku.hk; dennyfu@hku.hk; guoziyan@connect.hku.hk; ziyang.dong@hku.hk; mcwleong@connect.hku.hk; zardchim@connect.hku.hk; kwokkw@hku.hk).

A. P.-W. Lee is with the Prince of Wales Hospital, The Chinese University of Hong Kong, Hong Kong (e-mail: alexpwlee@cuhk.edu.hk).

W. Luk is with the Department of Computing, Imperial College London, London SW7 2AZ, U.K. (e-mail: w.luk@imperial.ac.uk).

This paper has supplementary downloadable material available at http://ieeexplore.ieee.org, provided by the author. The material is one video clip, 74 MB, showing the catheter robot.

Color versions of one or more of the figures in this paper are available online at http://ieeexplore.ieee.org.

Digital Object Identifier 10.1109/TMECH.2018.2801787

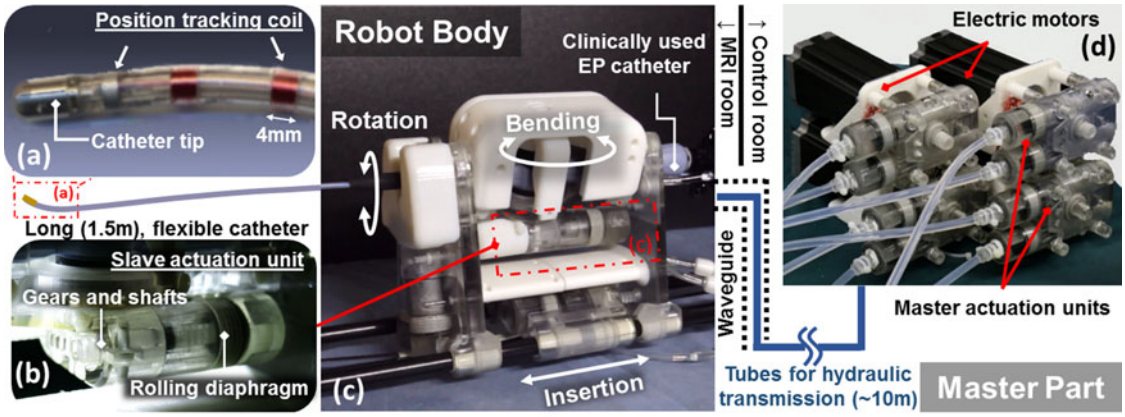

Fig. 1. Overview of the MR Safe hydraulic catheter robotic manipulator showing the allocation of master–slave actuation in MRI room setting. (a) Two small active tracking coils wired along the catheter for real-time positional MR tracking of its tip. (b) The MR Safe robotic platform plugged-in with a standard EP catheter for RF ablation. The master–slave actuation units provide rotation, bending, coarse, and fine insertion of the catheter. (c) Bending actuation unit that transmits the linear hydraulic actuation of rolling diaphragm into rotary motion. All hydraulic actuation units and the robot body are made of MR Safe materials. (d) Master electric motor units located in the control room serving as the source of hydraulics. The hydraulic fluid is transmitted to the slave catheter robot platform in MRI room via long (≈10 m) hydraulics pipelines. These hydraulics tubes can be channeled through the waveguide.

Despite the significant benefits of robot-assisted catheterization as well as the advances of intra-op MRI, no existing commercial robotic catheterization platform is MR compatible. The main contribution of this paper is the development of an MR Safe robotic manipulator (see Fig. 1) for intracardiac catheterization. Detailed design features and its hydraulic actuation mechanism are described (see Section II) together with experimental evaluations (see Section III) for telemanipulation of a clinically used catheter. We also review some state-of-the-art enabling techniques for MRI-guided intervention assisted by teleoperated robots (see Section IV). Demonstration of the basic robot components and the integrated control interface for MRI-guided EP is also highlighted in the attached video.

II. Design of MR Safe Robotic Components

Fig. 1 illustrates the key components of the proposed MR Safe robotic manipulator. Such system has to comply with four major design requirements for clinical application.

R1) The robot operation must not pose any hazard to the patient and to the MRI scanner, and does not adversely affect the quality of MR images.
R2) The robot has to be compatible with clinically used catheter and the corresponding 3-D cardiovascular navigation system.
R3) The robot can enable precise actuation with sufficient degrees of freedom (DoFs) to carry out intracardiac catheterization, comparable to manual control of the catheter.
R4) The robot should be compact, light-weight, and easy to sterilize.

The key robotics components to fulfill these requirements are proposed in the following sections.

A. Master–Slave Hydraulic Actuation Units

In MRI environments, electromagnetic (EM) and electrically conductive components have to be handled with caution. Any electric current would inevitably induce EM interference that disrupts the magnetic or gradient field homogeneity in MRI scanner, deteriorating the image quality. This poses a significant challenge to adopt EM motors in actuation mechanism design, particularly for precise catheterization. A common approach is to isolate the motors with complex EM-shielding within the MRI room. However, it is still technically difficult to filter out high-frequency control signals without affecting motor operation and design compactness. Recently, an advanced design on piezoelectric motor has been shown to reduce signal-to-noise ratio (SNR) loss to less than 15% using high-frequency signal transmission [8]. To this end, we aim at developing intrinsically MR Safe and fluid-driven actuators, so that no EM material/power will exist in the MRI room. Previous examples are the MR Safe pneumatic stepper motor presented in [9] and [10] and the MR Safe pneumatic needle-guide robot [11].

To address R1), master–slave hydraulic transmission is adopted in the design of actuation units (see Fig. 2) to drive a catheter. In contrast to pneumatic actuation, hydraulic actuation uses incompressible fluid as working media, offering more steady transmission and quicker response. In the proposed robot, each master unit is actuated by an electric dc motor located in the control room. Each slave unit operates on the patient table near the MRI scanner. Such separation ensures negligible EM interference to the MR images, and allows the compact design of the slave units. During operation, each master unit drives the corresponding slave unit and subsequently the catheter, via two long pipelines (≈10 m each) through the waveguide in-between the control room and the to achieve efficient transmission, rolling diaphragms [12] are employed to seal every master and slave actuation units (see Fig. 2). Compared to the sealing approaches using O-ring, rolling diaphragms can offer effective sliding with negligible friction between the piston and the inner wall of the cylinder, thus reducing energy loss during actuation. This kind of elastomeric sealing is made of MR Safe, nonmetallic material reinforced by fabric to withstand the high internal fluid pressure.

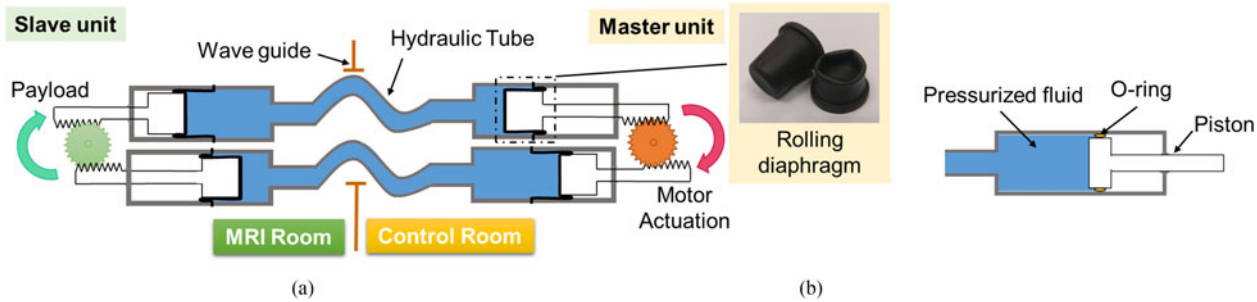

Fig. 2. (a) Conceptual design of master–slave hydraulic transmission to ensure MR compatibility of robot actuation. The contact between the gear teeth can be maintained by preloading fluid pressure, thus minimizing backlash. Rolling diaphragms are adopted to tightly seal the pressurized fluid. (b) Conventional sealing using O-rings may induce significant sliding friction inside the cylinders.

TABLE I
SPECIFICATIONS OF THE MR SAFE MANIPULATOR

Size	$780 \times 105 \times 210\,\text{mm}^3$
Weight	3.16 kg (The whole slave body)
Hydraulic pipelines	Length: ≈ 10 m; Outer/Inner diameter: 6/4 mm (Nylon: DG-5431101, Daoguan Inc,)
Transmission media	Pressurized ($\leq$0.3 MPa) distill water
Rolling diaphragms	Diameter: 18 mm; Stroke length 35 mm (MCS2018M, FEFA Inc.)
Power source	Four dc motors with 500 pulses encoder(Maximum torque 278 mN·m; Gear ratio 14:1, HFmotor-40150, Chengdu Hangfa Hydraulic Engineering Co., Ltd)
Range of motion:	(Equivalent motion to encoder resolution)
Steering	$-45^\circ \leq \theta_s \leq 45^\circ$ (0.063°)
Rotation	$-360^\circ \leq \theta_r \leq 360^\circ$ (0.504°)
Coarse translation	$0\,\text{mm} \leq d_c \leq 200\,\text{mm}$ $(0.115\,\text{mm})$
Fine translation	$0\,\text{mm} \leq d_f \leq 30\,\text{mm}$ $(0.016\,\text{mm})$

The slave actuation would be lagged behind the master input, for example, caused by the backlash between gears or long hydraulic transmission via flexible pipelines. This lagged phenomenon is known as hysteresis that may significantly affect the performance of the catheter robot. The gear backlash can be reduced by loading higher pressure inside the pipelines such that the pressurized fluid always pushes the pistons toward the gears, thereby keeping the teeth in contact (see Fig. 2). The effects of preloading pressure on the robot's dynamic performance are experimentally analyzed in Section III.

B. Catheter Robot Design and Structure

To address R3), the robot employs *four* pairs of the master–slave actuation units (see Fig. 3), providing steering, rotation, coarse, and fine translation of the catheter with sufficient motion ranges (see Table I). The coarse and fine translation DoFs enable, respectively, the longer journey navigation from vessels to the heart chambers, and the shorter range of dexterous tip movement inside the heart chambers for EA mapping and delicate RF ablation. Because the stroke lengths of the rolling diaphragms are limited, the ranges of motion at the rotation and the coarse translation DoFs are magnified using gearboxes at the corresponding slave units. The coarse translation DoF is belt-driven and shares the same moving axis with the fine translation DoF. The steering angle of the catheter tip depends on the choice of the catheter. For example, the Thermocool Smarttouch Bi-Directional Catheter (Biosense Webster Inc.) can be steered up to 180° in two directions.

To address R2), the angular positions of the master gears can be precisely controlled (see Table I) using the motors' built-in proportional-integral derivative (PID) controllers. Since pipeline diameter and length also contribute to the fluid dynamics [13], stiff pipelines made of nylon (see Table I) are employed to minimize the pipe deformation when subjected to transmission force, thereby maintaining high precision output at the slave gears.

The modularized catheter holders [see Fig. 3(a)] can be tailor-made for various kinds of steerable EP catheters (e.g., Biosense Webster Inc. or St. Jude Medical). It allows switching between different catheterization systems simply by replacing the detachable catheter holders. A "plugging-in" mechanism is also designed to facilitate fast and reliable replacements. These catheter holders can be 3D-printed to account for future upgrades of any new catheter handle design.

To minimize the EM interference to the MR images, all the components of the slave system are made of MR Safe materials. Nonconducting, nonmetallic, and nonmagnetic items may be determined to be MR Safe by providing scientifically based rationale rather than test data [14]. The main structural components are 3D-printed using acrylic compounds (VeroWhitePlus/VeroClear, Stratasys, USA). The key actuation components include gears made of nylon, a transmission belt made of rubber, and auxiliary parts made of polymers [e.g., Polyvinyl Chloride (PVC), Polyetherimide (PET)]. This master–slave system has been tested to withstand rapid actuation ($\leq$15 Hz) under high fluid pressure ($\leq$0.3 MPa). To address R4) regarding sterilization, this small-sized slave body can be enclosed by disposable surgical equipment drapes. The insertion guide (see Fig. 3) made of low-cost acrylic compounds is also disposable and can be sterilized beforehand.

III. EXPERIMENTAL PERFORMANCE EVALUATION

To validate the robot performance for MRI-guided robot-assisted catheterization, we have conducted the following.

1) An MRI-compatibility test.

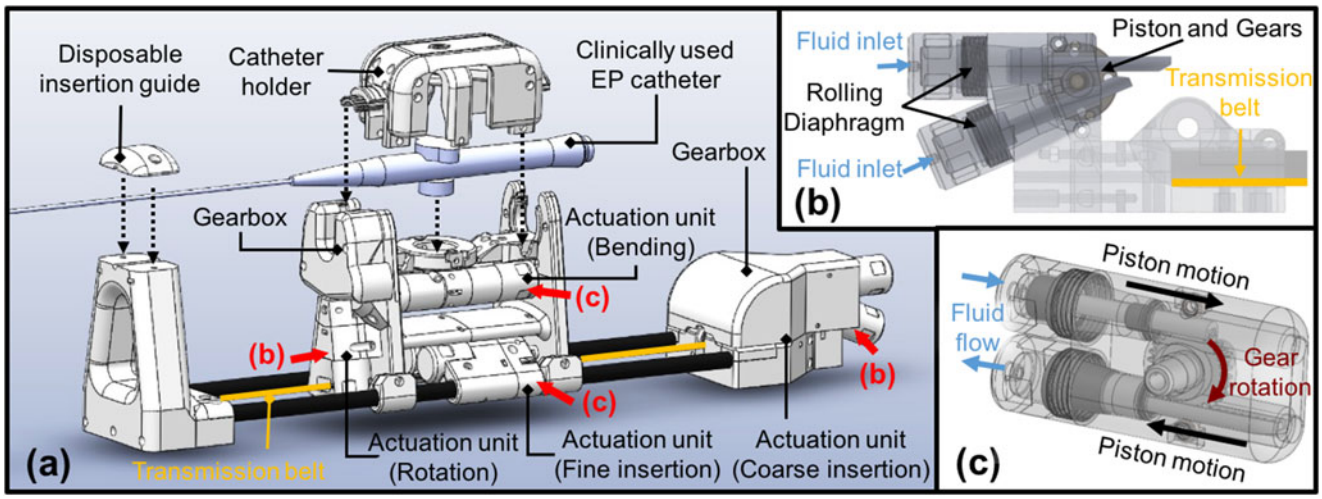

Fig. 3. (a) Main components of the MR Safe robotic manipulator (the slave system), which operates in the MRI room. A clinically used EP catheter can be tightly mounted on a tailor-made catheter holder. (b) and (c): actuation units providing steering, rotation, coarse, and fine translation of the catheter.

2) Performance analyses of the master–slave hydraulic actuators.
3) A lab-based simulated ablation task on a LA phantom model.

A. MR-Compatibility Test

The slave robotic manipulator placed in MRI room complies with the MR Safe classification of American Society for Testing and Materials (ASTM) standard F2503-13 [14], in which the robot comprises solely nonconducting, nonmetallic, and nonmagnetic materials. For the safety concerns of experiment, some components were double confirmed using metal/magnetic detectors before their integration. We simulated the basic operation for testing the compatibility with the MRI [see Fig. 4(a)]. The master system was actuated inside the control room inside a 1.5 T MRI scanner (SIGNA, General Electric Company, USA). The slave system was placed adjacent to a standard MRI phantom (J8931, J. M. Specialty Parts, USA) filled with distilled water. The phantom was placed at the isocenter of the scanner, and then imaged to evaluate the potential EM interference generated by the slave robotic manipulator.

Fig. 4(b) depicts the resulting MR images of the phantom under four different conditions.

1) *Phantom*: Only the phantom alone was placed in the scanner.
2) *Static*: The robot was introduced and remained power OFF.
3) *Powered*: The robot was kept still, but with the hydraulic and electric power ON in the control room.
4) *In motion*: The robot was in operation, manipulating the EP catheter.

Condition i) serves as the baseline for evaluation. The EM-induced effects on the MR images were measured based on the changes in the SNR $J = I/\sigma$, where I is the mean intensity value of a 40×40 pixels region at the image center, and σ is the standard deviation of intensity value in a region of 40×40 pixels at the lower right corner [15]. The MR images had maximum SNR loss less than 2% and had no observable image artifacts during the robot operation.

B. Hydraulic Transmission Performance

In the proposed master–slave actuators, the hydraulic transmission fluid was prepressurized in order to diminish the hysteresis due to gear backlash or the long ($\approx$10 m) hydraulic transmission (see Section II-A). However, the excessive preload pressure also led to severe gear and pivot friction, which may in turn degrade the manipulation precision. In this section, we first evaluated the force transmission performance, and then analyzed the position tracking accuracy and the effects of preload fluid pressure on the hysteresis, as well as on the resultant dynamic performance.

1) Force Transmission: The force transmission performance of the master–slave actuator is evaluated with a free weight-lifting experiment. In this experiment, a rotary slave actuator depicted in Fig. 1(c) is coupled to a winch of 5-cm radius. With the hydraulic fluid preloaded at 0.1 MPa, the master–slave actuator is capable of lifting 3 kg at a constant velocity of 10.01 cm/s, corresponding to an output torque of 1.47 N·m and net power of 2.93 W. The input torque at the motor axis on master side is also monitored by a torque sensor, which is used to estimate the hydraulic force transmission efficiency as 70%. Such force transmission performance is more than sufficient to steer the rotor on the standard catheter handle in full range, to roll the catheter ($>360^\circ$), and also to push/pull the catheter (<230 mm) through the introducer sheath and the guiding tube.

In fact, the maximum torque of the present prototype is limited by the mechanical strength of the 3D-printed components. In the real practice for human trials, the robot prototype ought to be fabricated with standard industrial machining procedures. Wider choices of MR Safe materials, such as Acetal (POM) or Nylon or any strong resilient plastic, will be used to comprise

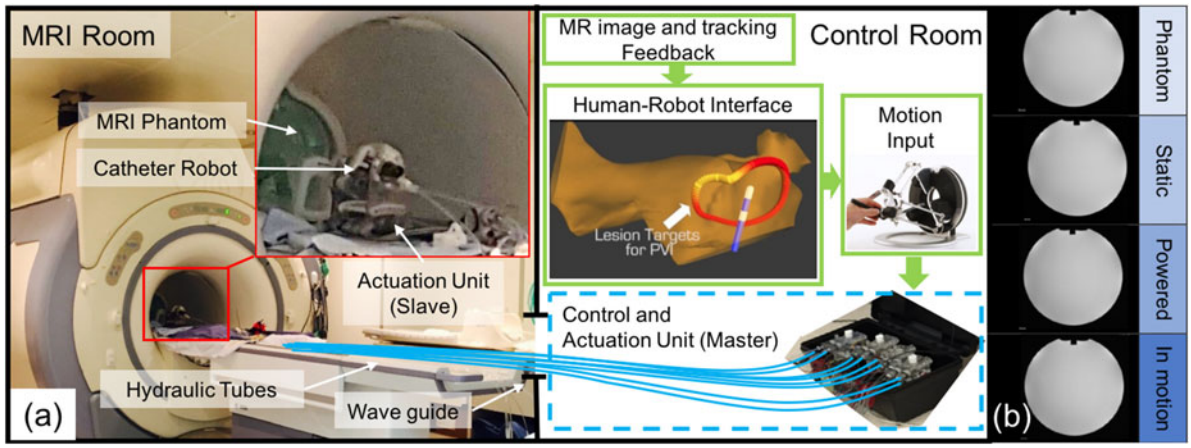

Fig. 4. (a) Experimental setup of MR-compatibility test for the presented robot. Key components are connected between the MRI and the control rooms via the wave guide. The operator can telemanipulate the catheter using the catheter navigation interface. (b) MR images of an MRI phantom placed aside the robot indicate the negligible EM interference in four different operating conditions.

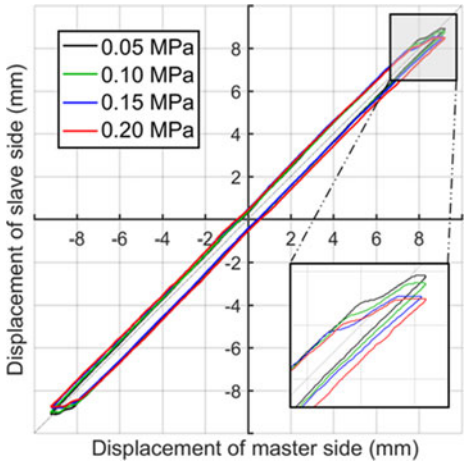

Fig. 5. Hysteresis of the master–slave actuation unit at different preload fluid pressure. The average values of hysteresis were 0.88 mm, 0.93 mm, 1.02 mm, and 1.29 mm for preloaded pressure 0.05 mPa, 0.1 mPa, 0.15 mPa, and 0.2 mPa, respectively.

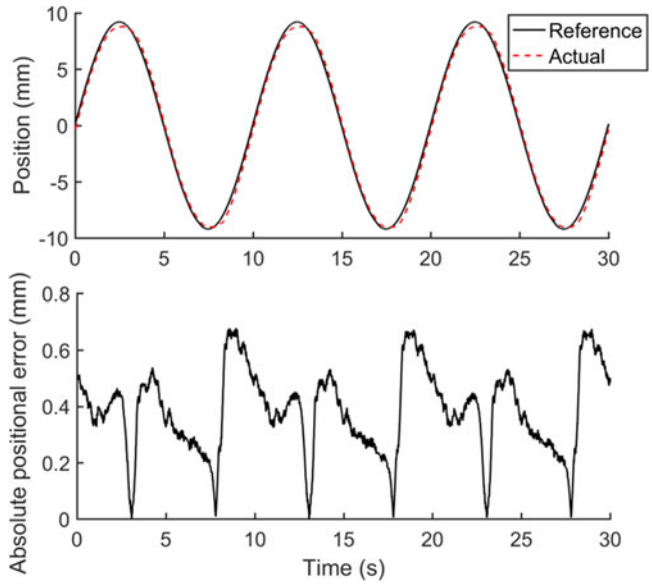

Fig. 6. Periodic motion of the master–slave actuation unit preloaded with 0.1 mPa of fluid pressure. The slave position (dash line, upper plot) could precisely follow the sinusoidal reference trajectory (concrete line, upper plot) of the master unit at 0.1 Hz. The absolute error (lower plot) has a maximum of 0.67 mm.

more robust structure for promising durability and enhanced actuation torque.

2) Hysteresis: Hysteresis is the primary concern for intracardiac intervention that requires accurate manipulation of the catheter with high resolution. The hysteresis of the pair of master–slave actuation units was measured and shown in Fig. 5. The translational positions of the master and slave pistons were measured at different levels of preloaded fluid pressure inside the pipelines. The periodic motion of the master unit was controlled by the embedded PID positional controller at a frequency of 0.1 Hz, where 70% of the stroke-length was covered. Fig. 6 depicts that the slave actuation unit could precisely follow a sinusoidal trajectory of the master unit, with a maximum absolute error of 0.67 mm. The hysteresis was largely uniform throughout the whole range of motion, particularly at higher preloaded pressure. The hysteresis only slightly increases with the preloaded pressure, potentially due to the rise in static friction between the gears.

3) Dynamic Response: The dynamic performance of the master–slave actuation units for different values of preloaded fluid pressure was investigated using a frequency response method. Given a sinusoidal torque input $\tau = A\sin(\omega t)$ to the master gear, where ω was the frequency and t was the time, the torque at the slave gear was measured. The amplitude A was set to 0.1 N·m, which is within the nominative operation range of the motor. Fig. 7 depicts the Bode plot that characterizes the "magnification" M and the "phase shift" ξ of the hydraulic transmission at steady state. Note that for a linear time invariant system, the frequency response at steady state becomes $\tau_{ss} = MA\sin(\omega t + \xi)$.

The magnitude plot indicates that the magnification increases with the preloaded fluid pressure. The magnification value peaks

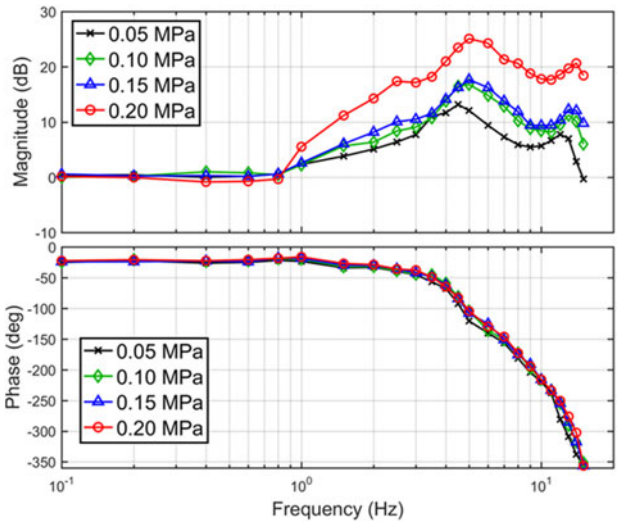

Fig. 7. Bode plot showing torque transmission response of the master–slave hydraulic actuation unit at four different levels of preloaded fluid pressure. The magnitude (top) and phase shift (bottom) are shown. The data were collected from ten cycles at the steady state.

at around 5 Hz, which corresponds to the natural frequencies of the overall hydraulic transmission. We also found that the increase of the preloaded fluid pressure does not significantly affect the natural frequency.

The phase lag of the transmission was kept at around 25° for low actuation frequency (<1 Hz), and was not significantly affected by the variation of the preloaded fluid pressure. The transmission had small time delay: 45 ms and 66 ms at actuation frequency 1 Hz and 15 Hz, respectively, with preloaded fluid pressure 0.2 mPa. Such phase shift and the natural frequency could result from the compliance of the 10 m long nylon tubes, rolling diaphragms. However, the actual transmission performance also depends on the complicated fluid dynamics, it will require further investigations based on dynamic modeling techniques to explain for the frequency response.

In summary, the master–slave actuator had small (1.29 mm at 0.1 Hz) hysteresis and quick response (66 ms at 15 Hz), even at a high preloaded fluid pressure (0.2 mPa). Although the increase of the preloaded fluid pressure slightly increased the hysteresis (from 0.88 mm at 0.05 mPa to 1.29 mm at 0.2 mPa), it could attain effective force transmission as shown in the Bode plot (see Fig. 7). As a result, it demonstrates that acceptable system delay could be maintained in a normative operating frequency for catheterization. Apart from the preloaded fluid pressure, fluid properties such as mass and viscosity would also affect the transmission. We employed distilled water as hydraulic fluid due to its ease of implementation and availability. The hydraulic pipelines length and diameter are also part of design considerations in regard to actuation dynamics. Previous analytical studies and experimental investigations [13] have suggested that the fluid friction can be reduced by using pipelines with a larger diameter, resulting in better system efficiency and smaller transmission phase lag. In addition, shorter pipelines are also preferable, which could reduce the transmission fluid inertia and also increase the transmission stiffness.

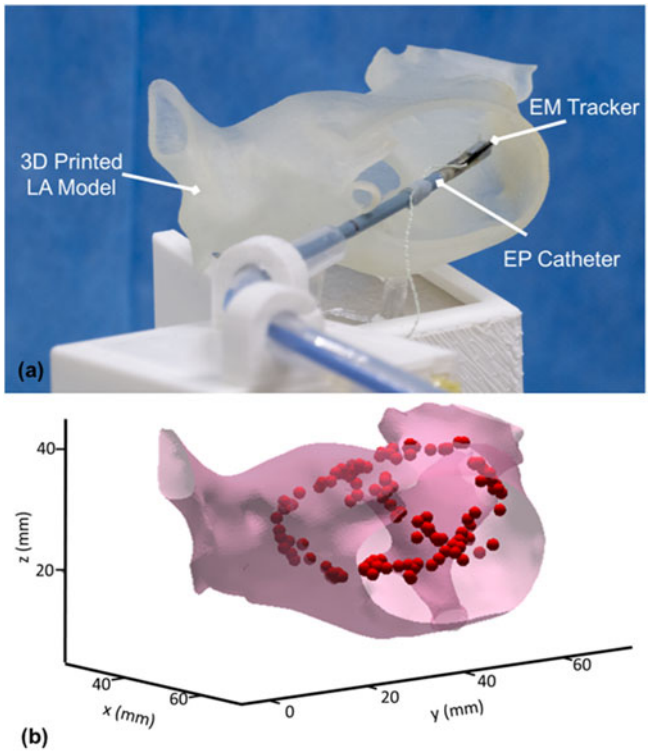

Fig. 8. (a) Experiment settings of the PVI task. A catheter was telemanipulated by the proposed robot to perform "ablation" on the LA phantom model. (b) Locations of the ablations (127 points) on the interior surface.

C. Catheter Manipulation for Pulmonary Vein Isolation

The robotic catheterization performance was validated by a simulated task of pulmonary vein isolation (PVI), which is a treatment of atrial fibrillation (AF). PVI requires RF ablation conducted inside the LA. A typical task is to make lesion scars along the ostia of the left superior and inferior pulmonary veins. Such consistent scars would isolate the abnormal electrical signal originated from the arrhythmias, which causes the irregular heart motion [16].

In our lab-based validation, a standard EP ablation catheter (Thermocool Smarttouch Bi-Directional Catheter, Biosense Webster Inc.) was "plugged-in" to the slave robot. An EM positional sensor (NDI Medical Aurora) was attached close to the catheter tip in order to track the 3-D tip positions in real time. The phantom LA was a 3D-printed model made of soft material (AgilusClear, Stratasys Inc.) according to real anatomical data. In this task, the subject could telemanipulate the catheter mounted on the robot using a motion input device (Novint Falcon, NF1-L01-004). He/she was advised to press the foot pedal, then activate the "RF ablation," once being able to confirm the proper tip contact with the lesion targets prescribed on the virtual LA model. Note that the 3-D tracking coordinates, along with the virtual model, have to be well aligned with the actual LA phantom [see Fig. 8(a)].

A reachability test was conducted with the aim to verify if the catheter tip driven by the presented robot is capable to reach or cover the region of interest along the ostia of the left superior and inferior pulmonary veins. Fig. 8(b) depicts the measured

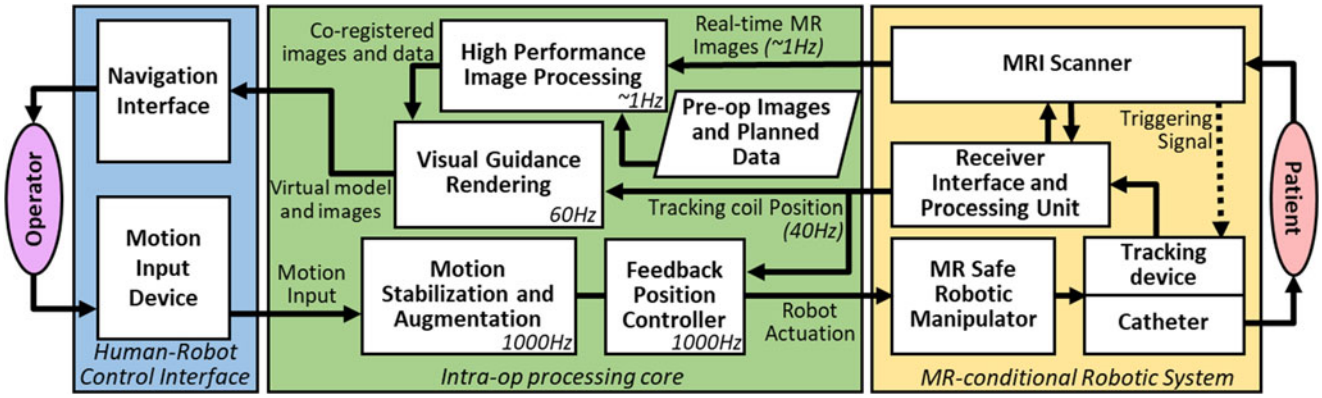

Fig. 9. Schematic diagram of the MRI-guided robot-assisted catheterization. The operator can perform robotic EP catheterization in a closed-loop manner.

footprint of the catheter tip along the ostia, which are the ablation points confirmed by the operator during the telemanipulation. Note that the robot catheterization precision should be taken into account, only if having detailed kinematic/dynamic study of the catheter itself. Such a study currently lies beyond the scope of this paper. In the real MRI-guided EP, such real-time 3-D tracking of the catheter can be achieved by MRI, also in the same image coordinate frame. Further details are discussed in Section IV.

IV. Toward MRI-Guided and Robot-Assisted Catheterization

Apart from the robot hardware, accurate MR-based localization of the catheter, as well as high-performance image registration, is of importance to realizing intra-op MRI-guided EP catheterization. In this section, MR-tracking and intra-op image registration techniques are reviewed. We also discuss the prospective integration of these two components into a human-robot control interface, which will enable a closed-loop control of the proposed robot under MRI. Fig. 9 illustrates this closed-loop architecture.

A. Real-Time Positional Tracking in MRI

Tracking the catheter position is essential in many cardiac interventions. This positional feedback data will close the control loop of robotic navigation (see Fig. 9). MR-based tracking can be achieved by attaching two tiny solenoid coils (see Fig. 1) close to the catheter tip, which are connected to a receiver electronic system via coaxial cables. This is a typical MR-*active* tracking setting, in which the coil can actively "pick up" the MR gradient field [17] along the three principal directions for localization. By matching/tuning the receiver's *LC* components for a specific MRI scanner, these coils can be highly sensitive to very local field inhomogeneity [18] without adversely affecting the image quality, providing high-resolution $(0.6 \times 0.6 \times 0.6\ \text{mm}^3)$ tracking performance with fast sampling rate (40 Hz) [19].

In contrast, the conventional use of *passive* MR fiducial markers is found to be difficult in achieving responsive/continuous tracking. Complicated MRI sequence is required, taking significant time to process susceptibility artefacts in the high-resolution images for fast and accurate localization. Recently, paramagnetic markers can be automatically localized at high frequency (50 Hz), but with a relatively large positional error of $\leq$4.5 mm when the MRI sequence PRIDE was used to acquire echo-phased projection in three principal axes [20].

MR-*semiactive* tracking is a state-of-the-art approach, in which coils are integrated into small isolated *LC* circuits. These coils resonate with specific MR frequencies by means of wireless inductive coupling with the MRI system. There are no direct capacitive electrical connections with the MRI system. This avoids resonating RF waves along the coaxial cables connection, which can pose potential heating hazard in active tracking (see Table II). Using a properly programmed MR sequence that detunes/triggers the isolated resonant circuit, the semiactive device can be visualized in the MR images. To alter the RF resonant behavior, an optical fiber could be connected to the circuit in order to illuminate a photodiode placed parallel to a coil, which could achieve real-time imaging (20 fps) in an *in vivo* test [21].

MR tracking also allows real-time visualization of the catheter configuration with respect to the EP roadmap constructed from the MR images. This could provide the operator with reliable navigation guidance and consistent motion reference to aim the catheter tip at the ablation lesions imaged and registered locally around the tip (see Fig. 4). Such intra-op visualization will involve fast image registration, which is described in the next section. A demonstration can be found in the attached video.

B. Intra-op MR Image Registration

With zero EM interference accredited to the proposed MR Safe hydraulic actuators, fast MR images can be acquired in the region around the catheter tip being tracked. Thus, the postablation lesions (edema or scars) can be promptly visualized and selected on T2-weighted MR images. These physiological changes need to be instantly overlaid on the EP roadmap, allowing the electrophysiologist to determine whether the ablation is applied sufficiently to the lesions. However, such intra-op MR images are mostly obtained at different cardiac cycles from the preoperative (pre-op) images that construct the EP roadmap. Nonrigid

TABLE II
TECHNOLOGIES REVIEWED FOR POSITIONAL TRACKING IN MRI

	Operating principles	Advantages	Disadvantages
Passive tracking	- Encapsulated –ve/+ve contrast agents causing MR signal void or T1 shortening. - Encapsulated materials visible by nonproton multispectral	- Simple and safe integration - Capable of operating under different field strengths	- Time consuming - Tracking cannot be switched ON/OFF
Active tracking	- Use image sequence to induce position-dependent MR gradient field within a volume of interest - Detect the MR gradient field using micro coil/antenna in frequency domain	- High spatial and temporal resolution of 3-D tracking information - Easy to conduct automatic tracking and slice plane following	- Potential risk of RF heating on wires connected to the receiver - Sophisticated tuning/matching the circuity in the required receiver interface
Semiactive tracking	- Isolated *LC* circuit with photodiode/photoresistor connected in parallel is designed to resonate at MRI Larmor frequency	- No electric wire connected with the scanner receiver - Optically controllable resonance behavior	- Difficulty in assembly and miniaturization - Sophisticated design of tracking sequence needed

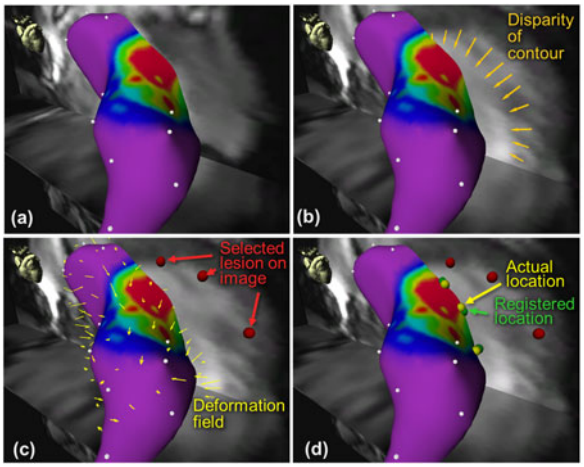

Fig. 10. (a) 3-D EP roadmap of LV segmented and rendered based on pre-op MR images. (b) Significant disparity (indicated by orange arrows) between the roadmap and intra-op images during the diastole. (c) Ablation landmarks selected on a slice of 2-D intra-op MR images. Yellow flow arrows are shown as the deformation field estimated by the Demons-based registration method. (d) The landmarks realigned appropriately on the 3-D roadmap based on the deformation field.

image registration is the prerequisite to continuously realign the selected lesion on the EP roadmap (see Fig. 10).

Intensity-based registration methods are usually employed, given the advantage of its higher tolerance of MR image noise and artifact, compared to the feature-based methods. *Diffeomorphic demons* [22] is a typical intensity-based approach, however, the computation is usually intensive. For example, our computer system currently takes 2 min and 30 s to process two sets of MR images with size of $256 \times 256 \times 181$ pixels. However, prolonged computation time required to align the target lesions frequently with the roadmap will undoubtedly hinder the surgical workflow. We have proposed that this computation bottleneck can be resolved using high-performance computing architectures [23], [24], such as graphical processing units (GPUs). GPUs facilitate spatial parallelism by simultaneously sharing the computation load with thousands of its processing units under the "Single instruction, multiple data" architecture. Vectorized data types (e.g., float4) by cascading multiple primitive data (e.g., 32-b float) also allow full utilization of the memory bus in GPU, as well as batch processing of multiple data under a single instruction.

Reconfigurable computing technology, such as field-programmable gate arrays (FPGAs), can also be employed to accelerate image registration and related applications. FPGAs' flexible architecture can effectively exploit temporal parallelism by customizing stream processing pipelines [25]. Furthermore, the bit-width of the data streams in FPGAs can be optimized based on tradeoffs between computation speed and accuracy. As a result, coregistration between two sets of 3-D images ($192 \times 132 \times 300$ pixels) could be achieved within 1.1 s [24]. Such rapid realignment of the intra-op image is crucial to achieving precise catheter manipulation in dynamic surgical scenarios. This fast MR registration would offer effective visual guidance in the human–robot control interface (see Fig. 4) that will be incorporated into our proposed robotic manipulator. Other robot motion planning tasks such as proximity query can also be accelerated by FPGAs [26].

C. Human–Robot Control Interface

Intra-op imaging can be applied in conjunction with MR tracking, such that the tracking is interleaved with the MR image sequence. This tracking involves measurement of both 3-D position and orientation of the catheter tip. These data can be continuously streamed to the EP navigation system and the robot control interface [27]. Note that the entire MR-based catheter tracking takes place in the same MR imaging coordinate system. Unlike conventional EP, our MR-based approach does not require external tracking reference, thereby avoiding potential disparity caused by relative registrations between tracking and imaging system. This enables rendering of the virtual endoscopic view from the viewpoint of the catheter tip [28]. Such virtual view facilitates fine placement of the catheter tip while approaching ablation targets registered on the roadmap (see Fig. 4). Moreover, robotic control methods that account for the catheter's kinematics/dynamics [29] could also be applied to provide the operator with a consistent manipulation reference upon this 2-D endoscopic view, as demonstrated in our attached video.

V. Conclusion

The proposed MR Safe robotic manipulator is the first of its kind that offers sufficient DoFs to telemanipulate a cardiac catheter under intra-op MRI guidance [30]. The robot fulfills the MR Safe standard (ASTM F2503-13), as it solely comprises nonconductive, nonmetallic, and nonmagnetic materials. Currently, there is no such commercial system that is MR compatible/conditional.

The proposed highly efficient hydraulic transmission using rolling diaphragm has been shown to have great potential for offering high-performance actuation under MRI without adversely affecting imaging quality (SNR loss $<2\%$). This master–slave actuation system involves an advanced sealing method, which has demonstrated its advantages in low-friction, quick-response and low-noise motion transmission. The slave actuation unit can output torque up to 1.47 N·m with a force transmission efficiency of 70%. Such actuation torque can be transmitted from the control room into the MRI room via 10 m long hydraulics pipelines that are channeled through the waveguide, while maintaining a small overall mechanical backlash of 0.88 mm by applying appropriate hydraulic pressure at 0.05 mPa. The incompressibility of hydraulic fluid also results in stable and low-latency dynamic response ($<$70 ms), even at high-frequency motion (15 Hz). The proposed manipulator is capable of performing a simulated PVI procedure, demonstrating its sufficient workspace and dexterity for EP catheterization.

Our ongoing work is to improve hydraulic actuation to offer a full range of catheter advancement along the vessels to the chamber. Furthermore, MR-tracking and intra-op image registration techniques are also essential to realize MRI-guided EP catheterization. Advanced MR-tracking devices can be used to localize the catheter tip at high frequency (40 Hz) and resolution ($0.6 \times 0.6 \times 0.6\,\text{mm}^3$) in the image coordinates, thus enabling accurate alignment of catheter configuration with the roadmap. Fast image registration implemented on advanced GPU/FPGA-based architecture can rapidly register/realign ($\sim$1.1 s) the lesions on the pre-op EP roadmap. The RF ablation progress can then be frequently monitored by the intra-op MR images. It avoids manual coordination of such lesions on the MR images, which may not be consistent with the roadmap at different points of the cardiac cycle.

In summary, the advent of the proposed MRI-guided catheter robotic system will increase confidence to perform RF ablation completely while improving the safety of catheter navigation. As a result, it may reduce nerve damage, esophageal fistula creation, pulmonary vein stenosis, and stroke, as well as the chance of postprocedural disease recurrence (currently 30% in AF and 50% in ventricular tachycardia). This will contribute to justify the use of MRI while reducing the overall healthcare expenditure of the treatments.

References

[1] F. Morady, "Radio-frequency ablation as treatment for cardiac arrhythmias," *New England J. Med.*, vol. 340, no. 7, pp. 534–544, 1999.

[2] M. Haïssaguerre *et al.*, "Spontaneous initiation of atrial fibrillation by ectopic beats originating in the pulmonary veins," *New England J. Med.*, vol. 339, no. 10, pp. 659–666, 1998.

[3] E. J. Schmidt *et al.*, "Electro–anatomic mapping and radio–frequency ablation of porcine left atria and atrio-ventricular nodes using magnetic resonance catheter tracking," *Circulation, Arrhythmia Electrophysiology*, vol. 109, 2009, Art. no. 882472.

[4] R. Razavi *et al.*, "Cardiac catheterisation guided by MRI in children and adults with congenital heart disease," *Lancet*, vol. 362, no. 9399, pp. 1877–1882, 2003.

[5] R. C. Susil, C. J. Yeung, H. R. Halperin, A. C. Lardo, and E. Atalar, "Multifunctional interventional devices for MRI: A combined electrophysiology/MRI catheter," *Magn. Reson. Med.*, vol. 47, no. 3, pp. 594–600, 2002.

[6] S. R. Dukkipati *et al.*, "Electroanatomic mapping of the left ventricle in a porcine model of chronic myocardial infarction with magnetic resonance–based catheter tracking," *Circulation*, vol. 118, no. 8, pp. 853–862, 2008.

[7] A. N. Raval *et al.*, "Real-time MRI guided atrial septal puncture and balloon septostomy in swine," *Catheterization Cardiovascular Interventions*, vol. 67, no. 4, pp. 637–643, 2006.

[8] H. Su *et al.*, "Piezoelectrically actuated robotic system for MRI-guided prostate percutaneous therapy," *IEEE/ASME Trans. Mechatronics*, vol. 20, no. 4, pp. 1920–1932, Aug. 2015.

[9] D. Stoianovici, A. Patriciu, D. Petrisor, D. Mazilu, and L. Kavoussi, "A new type of motor: Pneumatic step motor," *IEEE/ASME Trans. Mechatronics*, vol. 12, no. 1, pp. 98–106, Feb. 2007.

[10] Y. Chen, K.-W. Kwok, and Z. T. H. Tse, "An MR-conditional high-torque pneumatic stepper motor for MRI-guided and robot-assisted intervention," *Ann. Biomed. Eng.*, vol. 42, no. 9, pp. 1823–1833, 2014.

[11] D. Stoianovici *et al.*, "Multi-imager compatible, MR safe, remote center of motion needle-guide robot," *IEEE Trans. Biomed. Eng.*, vol. 65, no. 1, pp. 165–177, Jan. 2018.

[12] J. P. Whitney, M. F. Glisson, E. L. Brockmeyer, and J. K. Hodgins, "A low-friction passive fluid transmission and fluid-tendon soft actuator," in *Proc. IEEE/RSJ Int. Conf. Intell. Robots Syst.*, 2014, pp. 2801–2808.

[13] G. Ganesh, R. Gassert, E. Burdet, and H. Bleuler, "Dynamics and control of an MRI compatible master-slave system with hydrostatic transmission," in *Proc. IEEE Int. Conf. Robot. Autom.*, 2004, vol. 2, pp. 1288–1294.

[14] Standard Practice for Marking Medical Devices and Other Items for Safety in the Magnetic Resonance Environment, ASTM International, West Conshohocken, PA, USA, ASTM F2503-13, 2013. [Online]. Available: www.astm.org

[15] K. Chinzei, R. Kikinis, and F. A. Jolesz, "MR compatibility of mechatronic devices: Design criteria," in *Proc. Int. Conf. Med. Image Comput. Comput.-Assist. Intervention*, 1999, pp. 1020–1030.

[16] H. Oral *et al.*, "Catheter ablation for paroxysmal atrial fibrillation," *Circulation*, vol. 108, no. 19, pp. 2355–2360, 2003.

[17] J. L. Duerk, E. Y. Wong, and J. S. Lewin, "A brief review of hardware for catheter tracking in magnetic resonance imaging," *Magn. Reson. Mater. Phys., Biol. Med.*, vol. 13, no. 3, pp. 199–208, 2002.

[18] A. Glowinski, G. Adam, A. Bücker, J. Neuerburg, J. J. van Vaals, and R. W. Günther, "Catheter visualization using locally induced, actively controlled field inhomogeneities," *Magn. Reson. Med.*, vol. 38, no. 2, pp. 253–258, 1997.

[19] W. Wang *et al.*, "Real-time active MR-tracking of metallic stylets in MR-guided radiation therapy," *Magn. Reson. Med.*, vol. 73, no. 5, pp. 1803–1811, 2015.

[20] S. Patil, O. Bieri, P. Jhooti, and K. Scheffler, "Automatic slice positioning (ASP) for passive real-time tracking of interventional devices using projection-reconstruction imaging with echo-dephasing (PRIDE)," *Magn. Reson. Med.*, vol. 62, no. 4, pp. 935–942, 2009.

[21] S. Weiss *et al.*, "In vivo safe catheter visualization and slice tracking using an optically detunable resonant marker," *Magn. Reson. Med.*, vol. 52, no. 4, pp. 860–868, 2004.

[22] T. Vercauteren, X. Pennec, A. Perchant, and N. Ayache, "Diffeomorphic demons: Efficient non-parametric image registration," *NeuroImage*, vol. 45, no. 1, pp. S61–S72, 2009.

[23] K. W. Kwok *et al.*, "Interfacing fast multi-phase cardiac image registration with MRI-based catheter tracking for MRI-guided electrophysiological ablative procedures," *Circulation*, vol. 130, Suppl. 2, 2014, Art. no. A18568.

[24] K. W. Kwok *et al.*, "FPGA-based acceleration of MRI registration: An enabling technique for improving MRI-guided cardiac therapy," *J. Cardiovascular Magn. Reson.*, vol. 16, no. S1, 2014, Art. no. W11.

[25] W. Atabany and P. Degenaar, "A spatiotemporal parallel image processing on FPGA for augmented vision system," in *Advances in Computer and Information Sciences and Engineering*. New York, NY, USA: Springer, 2008, pp. 558–561.

[26] T. C. Chau *et al.*, "Acceleration of real-time proximity query for dynamic active constraints," in *Proc. Int. Conf. Field-Program. Technol.*, 2013, pp. 206–213.
[27] Y. Feng *et al.*, "An efficient cardiac mapping strategy for radiofrequency catheter ablation with active learning," *Int. J. Comput. Assist. Radiol. Surg.*, vol. 12, no. 7, pp. 1199–1207, Jul. 2017.
[28] Y. Chen *et al.*, "Augmented reality for improving catheterization in magnetic resonance imaging-guided cardiac electrophysiology therapy1," *J. Med. Devices*, vol. 8, no. 2, 2014, Art. no. 020917.
[29] C. L. Cheung *et al.*, "Kinematic-model-free positional control for robot-assisted cardiac catheterization," in *Proc. Hamlyn Symp. Med. Robot.*, 2016, pp. 80–81.
[30] Z. Guo, Z. Dong, K.-H. Lee, D. K. Fu, and K.-W. Kwok, "Robotic catheter system for MRI-guided cardiovascular interventions," Patent US15/630,406; PCT/CN2017/089701, 2016.

Kit-Hang Lee received the Bachelor's degree in mechanical and automation engineering from The Chinese University of Hong Kong, Hong Kong, in 2011, and is currently working toward the Ph.D. degree in medical robotics at the Department of Mechanical Engineering, The University of Hong Kong, Hong Kong, since 2015.

He was the recipient of a Croucher Foundation Research Scholarship supporting his Ph.D. study. His main research interests include magnetic resonance imaging guided robotic interventional systems, high-performance computing for medical image processing, and soft-bodied robotics design and control.

Kin Chung Denny Fu received the M.Phil. degree in automation and computer-aided engineering from The Chinese University of Hong Kong, Hong Kong, and the Ph.D. degree in robotics from the Graduate School of Engineering Science, Osaka University, Osaka, Japan.

He was with the Group of Interventional Robotic and Imaging Systems in the Department of Mechanical Engineering, The University of Hong Kong, where he worked on various types of image-guided surgical robotic systems and soft robotic systems. His research interests include medical robotics, soft robotics, nonlinear control and machine learning.

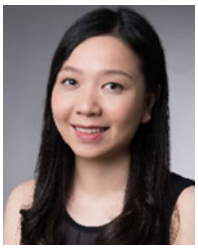

Ziyan Guo received the B.Eng. degree in automotive engineering from the Department of Automotive Engineering, Tsinghua University, Beijing, China, in 2013, and is currently working toward the Ph.D. degree in robotics at The University of Hong Kong, Hong Kong.

Her research interests include surgical robotics and image-guided interventions.

Ziyang Dong received the M.S. degree in mechanical engineering from The University of Hong Kong, Hong Kong, in 2015. Since 2016, he has been working toward the Ph.D. degree at the Group for Interventional Robotic and Imaging Systems, The University of Hong Kong, Hong Kong.

His research interests include surgical robotics, MR Safe/conditional robotic systems, and actuation design.

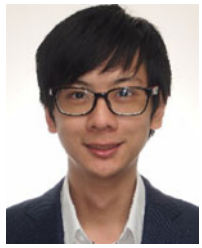

Martin C. W. Leong received the B.Eng. degree in medical engineering from The University of Hong Kong, Hong Kong, in 2015, where he is currently working toward the M.Phil. degree in medical robotics at the Department of Mechanical Engineering.

His research interests include high-performance computing architecture, graphical processing unit enabled nonrigid image registration, surgical simulation, and medical three-dimensional printing.

Chim-Lee Cheung received the B.Eng. degree in electrical engineering from The University of Hong Kong, Hong Kong, in 2015, where he is currently working toward the M.Phil. degree in medical robotics.

His research interests include the design and fabrication of intraoperative magnetic resonance imaging tracking devices for robot-assisted system.

Alex Pui-Wai Lee received the MD degree in cardiology from the Chinese University of Hong Kong (CUHK), Sha Tin, Hong Kong, in 2000. He is an Associate Professor with the Department of Medicine and Therapeutics, The Chinese University of Hong Kong, Hong Kong. He is an Academic Cardiologist specializing in cardiac imaging with particular interest in echocardiography. His main research interests include heart valve disease, heart failure, structural heart intervention, and biomedical engineering.

Prof. Lee has been the recipient of numerous awards, including the European Society of Cardiology Young Investigator Award and the State Ministry of Education First-Class Award in Technology Advancement. He is a Fellow of the American College of Cardiology, Royal College of Physicians of London, Hong Kong Academy of Medicine (Anaesthesiology), Hong Kong College of Pathologists.

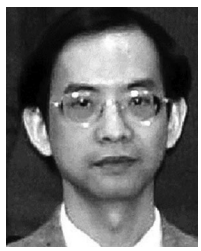

Wayne Luk (F'09) received the M.A., M.Sc., and D.Phil. degrees in engineering and computing science from Oxford University, Oxford, U.K. He is a Professor in computer engineering with Imperial College London, London, U.K.

His current research interests include theory and practice of customizing hardware and software for specific application domains such as genomics and climate modeling, and high-level compilation techniques and tools for high-performance computers and embedded systems.

Prof. Luk is a Fellow of the Royal Academy of Engineering and the BCS. He was the recipient of the Research Excellence Award from Imperial College London, and 11 awards for his publications from various international conferences.

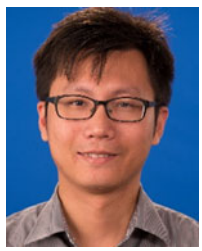

Ka-Wai Kwok received the Ph.D. degree from The Hamlyn Centre for Robotic Surgery, Imperial College London, London, U.K., in 2012.

He is an Assistant Professor with the Department of Mechanical Engineering, The University of Hong Kong, Hong Kong. His research focuses on robot systems for image-guided interventions.

Dr. Kwok's work has also been recognized by several awards from IEEE international conferences, including ICRA'17, ICRA'14, IROS'13, and FCCM'11. He also became the recipient of Early Career Awards 2015/16 offered by the Research Grants Council of Hong Kong.